Check for updates

Journal of Pathology
J Pathol May 2024; **263:** 61–73
Published online 9 February 2024 in Wiley Online Library
(wileyonlinelibrary.com) DOI: 10.1002/path.6260

ORIGINAL ARTICLE

Comprehensive clinicopathological, molecular, and methylation analysis of mesenchymal tumors with *NTRK* and other kinase gene aberrations

Natálie Klubíčková[1,2*†], Josephine K Dermawan[3†], Elaheh Mosaieby[1,2], Petr Martínek[2], Tomáš Vaněček[2], Veronika Hájková[2], Nikola Ptáková[2,4], Petr Grossmann[2], Petr Šteiner[2], Marián Švajdler[1,2], Zdeněk Kinkor[2], Květoslava Michalová[1,2], Peter Szepe[5], Lukáš Plank[5], Stanislava Hederová[6], Alexandra Kolenová[6], Neofit Juriev Spasov[7], Kemal Kosemehmetoglu[8], Leo Pažanin[9], Zuzana Špůrková[10], Martin Baník[11], Luděk Baumruk[12], Anders Meyer[13], Antonina Kalmykova[14], Olena Koshyk[14], Michal Michal[1,2] and Michael Michal[1,2]

[1] *Department of Pathology, Faculty of Medicine in Pilsen, Charles University, Pilsen, Czech Republic*
[2] *Bioptical Laboratory Ltd, Pilsen, Czech Republic*
[3] *Robert J. Tomsich Pathology and Laboratory Medicine Institute, Cleveland Clinic, Cleveland, OH, USA*
[4] *Department of Biology and Medical Genetics, Second Faculty of Medicine, Charles University and Motol University Hospital, Prague, Czech Republic*
[5] *Institute of Pathological Anatomy, Jessenius Faculty of Medicine in Martin, Comenius University, Martin, Slovakia*
[6] *Department of Pediatric Hematology and Oncology, National Institute of Children's Diseases and Medical Faculty, Comenius University, Bratislava, Slovakia*
[7] *Department of Pediatrics and Medical Genetics, Oncohematology Unit, Medical University Plovdiv, University Hospital Sveti Georgi, Plovdiv, Bulgaria*
[8] *Department of Pathology, Hacettepe University, Ankara, Turkey*
[9] *Department of Pathology, Sestre Milosrdnice University Hospital Center, Zagreb, Croatia*
[10] *Department of Pathology, Na Bulovce Hospital, Prague, Czech Republic*
[11] *Department of Pathology, Regional Hospital Karlovy Vary, Karlovy Vary, Czech Republic*
[12] *Department of Pathology, Regional Hospital Příbram, Příbram, Czech Republic*
[13] *Department of Pathology, University of Kansas, Kansas City, KS, USA*
[14] *Medical Laboratory CSD Health Care Ltd, Kyiv, Ukraine*

**Correspondence to: N Klubíčková, Department of Pathology, Medical Faculty and University Hospital Plzeň, Charles University, Alej Svobody 80, 323 00 Pilsen, Czech Republic. E-mail: klubickova@biopticka.cz*

[†]These authors contributed equally to this study.

Abstract

Alterations in kinase genes such as *NTRK1/2/3*, *RET*, and *BRAF* underlie infantile fibrosarcoma (IFS), the emerging entity '*NTRK*-rearranged spindle cell neoplasms' included in the latest WHO classification, and a growing set of tumors with overlapping clinical and pathological features. In this study, we conducted a comprehensive clinicopathological and molecular analysis of 22 cases of IFS and other kinase gene-altered spindle cell neoplasms affecting both pediatric and adult patients. Follow-up periods for 16 patients ranged in length from 10 to 130 months (mean 38 months). Six patients were treated with targeted therapy, achieving a partial or complete response in five cases. Overall, three cases recurred and one metastasized. Eight patients were free of disease, five were alive with disease, and two patients died. All cases showed previously reported morphological patterns. Based on the cellularity and level of atypia, cases were divided into three morphological grade groups. S100 protein and CD34 were at least focally positive in 12/22 and 14/22 cases, respectively. Novel *PWWP2A::RET*, *NUMA1::RET*, *ITSN1::RAF1*, and *CAPZA2::MET* fusions, which we report herein in mesenchymal tumors for the first time, were detected by RNA sequencing. Additionally, the first uterine case with *BRAF* and *EGFR* mutations and CD34 and S100 co-expression is described. DNA sequencing performed in 13 cases uncovered very rare additional genetic aberrations. The CNV profiles showed that high-grade tumors demonstrate a significantly higher percentage of copy number gains and losses across the genome compared with low- and intermediate-grade tumors. Unsupervised clustering of the tumors' methylation profiles revealed that in 8/9 cases, the methylation profiles clustered with the IFS methylation class, irrespective of their clinicopathological or molecular features.

© 2024 The Authors. *The Journal of Pathology* published by John Wiley & Sons Ltd on behalf of The Pathological Society of Great Britain and Ireland.

Keywords: *NTRK*-rearranged spindle cell neoplasms; infantile fibrosarcoma; kinase gene fusion; methylation profiling; *BRAF* mutation; entrectinib; larotrectinib; selpercatinib; *CDKN2A*

Received 7 August 2023; Revised 13 December 2023; Accepted 4 January 2024

No conflicts of interest were declared.

© 2024 The Authors. *The Journal of Pathology* published by John Wiley & Sons Ltd on behalf of The Pathological Society of Great Britain and Ireland. This is an open access article under the terms of the Creative Commons Attribution-NonCommercial-NoDerivs License, which permits use and distribution in any medium, provided the original work is properly cited, the use is non-commercial and no modifications or adaptations are made.

Introduction

Soft tissue tumors with kinase gene alterations comprise a heterogeneous group of mesenchymal neoplasms which includes, besides others, dermatofibrosarcoma protuberans (DFSP), inflammatory myofibroblastic tumor (IMT), and infantile fibrosarcoma (IFS) [1]. In addition to the canonical *ETV6::NTRK3* fusion described in IFS more than two decades ago [2,3], the recent widespread adoption of RNA sequencing (RNA-seq) has led to the description of several alternative gene rearrangements such as those of *NTRK1/2/3*, *BRAF*, *MET*, and others [1,4–7]. It has also led to the emergence of a novel and not yet fully defined group of mesenchymal tumors with kinase gene alterations that partially overlaps with IFS. It is currently included in the WHO classification as '*NTRK*-rearranged spindle cell neoplasms' (*NTRK*-SCN) [8,9]. It includes spindle cell tumors of both children and adults that form a continuous morphological spectrum which, based on cellularity and degree of atypia, can be roughly divided into three morphological subgroups.

The first subgroup consists of bland spindle cell lesions exhibiting low cellularity, minimal atypia, and very few mitoses [further referred to as the low-grade (LG) group], while the second contains lesions with high cellularity, high mitotic activity, and a high level of atypia [high-grade (HG) group]. In addition, some cases are difficult to assign to one of these categories as they fall somewhere in-between [intermediate-grade (IG) group]. The LG group may exhibit one of several often co-occurring morphological patterns such as a lipofibromatosis-like neural tumor (LNT) pattern [10], a prominent stromal and perivascular hyalinization (SPH) pattern [11], a myopericytic/hemangiopericytic pattern [12], and others [9,13]. Tumors in the IG group may retain similar patterns, or they may vaguely resemble LG malignant peripheral nerve sheath tumors (LG-MPNSTs) [9,14]. Tumors from the HG group morphologically overlap with IFS, adult fibrosarcoma, and/or HG-MPNSTs (due to significant overlap, these will be collectively referred to as the IFS pattern) [1,9,14].

Many tumors across the morphological spectrum of *NTRK*-SCN exhibit immunohistochemical co-expression of CD34 and S100 protein, and their molecular background is characterized by various gene fusions of, and less often mutations in, kinase genes such as *NTRK1/2/3*, *BRAF*, *RAF1*, *RET*, *MET*, and others [9,14–22], all of which lead to the activation of the MAP kinase signaling pathway [1]. However, very little is known regarding their methylation and copy number variation (CNV) profiles and potential secondary genetic alterations. In this clinicopathological study, we focused on their comprehensive molecular characterization using FISH, DNA sequencing (DNA-seq), and RNA-seq, as well as CNV and methylation profiling.

Materials and methods

Compliance with ethical standards

The study was conducted following the rules set by the Faculty Hospital in Pilsen Ethics Committee. Informed consent was not required for the study.

Case selection

Twenty-two cases falling within the morphological and molecular spectrum of the so-called *NTRK*-SCN and IFS were retrieved from our institutional tumor registry. All but one were received in consultation, which explains the low incidence of conventional *ETV6::NTRK3*-fused IFS in our cohort. Cases 11, 16, and 18 were reported previously by our group but were now subjected to a more extensive molecular-genetic analysis [19,20,23]. In case 6, LG and HG areas were present in two different sections, which enabled us to analyze both parts separately. Based on cellularity (defined as no overlapping, partial overlapping, or consistent overlapping of tumor cells) and level of atypia (classified based on uniformity of tumor cells, nuclear to cytoplasmic ratio, and hyperchromatism of nuclei), the cases were divided into three morphological grade groups as outlined in the Introduction. Importantly, this division was based purely on morphological features and is not meant to imply clinical behavior of grade 3 (or HG) sarcomas.

Immunohistochemistry

All cases were immunohistochemically stained using a Ventana BenchMark ULTRA (Ventana Medical System, Inc., Tucson, AZ, USA) for S100 protein and CD34. Additionally, 12 cases that harbored *NTRK1/3* rearrangements were tested with a panTrk antibody. Details regarding antibody dilutions and clones are provided in supplementary material, Table S1.

Molecular genetic studies

All molecular methods in this section are described in more detail in Supplementary materials and methods.

FISH

For the detection of *CDKN2A* loss using FISH, factory premixed ZytoLight SPEC *CDKN2A/CEN9* Dual Color Probe (ZytoVision GmbH, Bremerhaven, Germany) was used. The FISH procedure was performed as described previously [24].

Next-generation sequencing (NGS)

The customized Sarcoma FusionPlex kit (ArcherDX Inc., Boulder, CO, USA) was used, which detects fusion transcripts of selected exons of 88 genes, and mutations in hotspots of 14 genes, respectively. For further mutation analysis, we used the commercially available TruSight Oncology 500 panel (Illumina, San Diego, CA, USA), a comprehensive NGS assay on FFPE samples that

© 2024 The Authors. *The Journal of Pathology* published by John Wiley & Sons Ltd on behalf of The Pathological Society of Great Britain and Ireland. www.pathsoc.org

10969896, 2024, 1, Downloaded from https://pathsocjournals.onlinelibrary.wiley.com/doi/10.1002/path.6260 by Ukraine - Cochrane, Wiley Online Library on [11/12/2024]. See the Terms and Conditions (https://onlinelibrary.wiley.com/terms-and-conditions) on Wiley Online Library for rules of use; OA articles are governed by the applicable Creative Commons License

identifies somatic variants, copy number changes, tumor mutational burden (TMB), and microsatellite instability (MSI). Only tumor tissue was analyzed, except for case 18 where a peripheral blood sample was available.

Methylation analysis

Eleven kinase-rearranged tumors were tested by methylation profiling (cases 1, 3, 4, 6, 11, 13, 15, 18, 19, 21, and 22). Two specimens failed quality control (cases 4 and 15). Genomic DNA was extracted from paraffin blocks and 250 ng of genomic DNA was subjected to bisulfite conversion and processed on the Illumina Infinium MethylationEPIC/850k platform (Illumina) with over 850,000 methylation sites according to the manufacturer's instructions.

Additionally, we obtained raw idat files for 247 samples from the Heidelberg sarcoma methylation classifier reference cohort (Gene Expression Omnibus study accession number GSE140668). Idat processing and data analysis on all 256 samples were performed using R software (version 4.1.0) (R Foundation for Statistical Computing, Vienna, Austria) and the 'minfi' R package (version 1.38.0) (Bioconductor, Boston, MA, USA).

For unsupervised clustering, dimensionality reduction was performed by the t-distributed stochastic neighborhood embedding (t-SNE) method. After normalizing the input data matrix (centering the mean of each column to zero), the top 10,000 most variable CpG sites by variance were analyzed using the 'Rtsne' R package (version 0.15) (https://CRAN.R-project.org/package=Rtsne, last accessed 8 June 2023) with the following nondefault parameters: perplexity = 10, max_iter = 5,000, and $\theta = 0$. Additionally, unsupervised hierarchical clustering was performed on the top 1,000 most variable CpG sites by variance using the 'pheatmap' R package (version 1.0.12) (https://CRAN.R-project.org/package=pheatmap, last accessed 8 June 2023) with Ward.D2's linkage and Euclidean distance for clustering.

For CNV analysis, the Mset files after idat files preprocessing were processed by the 'conumee' R package (version 1.32.0) (Bioconductor). CNV was considered present if the absolute segmentation mean was greater than or equal to 0.3. The fraction of CNV across the genome was calculated by dividing the sum of all segments with CNV by the sum of all segments across the genome. Additionally, the idat raw data files were uploaded to a DNA methylation-based classification tool, Sarcoma classifier (version 10.1) [25,26], available via https://www.molecularneuropathology.org/ (last accessed 8 June 2023).

Results

Clinical data

Clinicopathological data are summarized in Table 1. There were 11 female and 11 male patients, including 14 children ranging in age from newborns to 13 years (mean 24 months; median 5.5 months). The eight adult patients were aged 26–72 years (mean 47 years; median 44.5 years). Various superficial and deep sites were affected including the duodenal wall ($n = 1$) or the uterus ($n = 2$). The size ranged from 1.3 to 30 cm (mean 8.5 cm, median 5 cm).

Histological findings

Microscopically, the tumors were usually uncircumscribed, and some widely infiltrated into the surrounding tissues. The 22 cases exhibited various and often multiple morphological patterns and morphological grades. In this situation, the highest grade was assigned.

Five cases at the LG end of the morphological spectrum exhibited SPH and LNT patterns and were composed of uniform bland non-overlapping spindle cells that were dispersed in abundant stroma. The mitotic activity did not exceed two mitoses per 10 high-power fields (HPF; 2.4 mm^2). The tumor cells grew in sheets or cords around thick hyalinized vessels in the case of SPH or widely infiltrated into subcutaneous adipose tissue in the case of LNT (Figure 1A). Case 11 showed a myxoid SPH pattern composed mostly of epithelioid cells with abundant eosinophilic cytoplasm (Figure 1B) [23].

Three IG cases showed more polymorphism, hyperchromasia, and occasional overlapping of tumor cells, which were arranged haphazardly or in short fascicles. The cases resembled LG-MPNST (Figure 1C) or had an SPH (Figure 1D) or a myopericytomatous pattern (case 19). The latter case was composed of myoid spindle cells arranged in haphazard fascicles punctuated by prominent vasculature (Figure 1E,F). The mitotic activity was higher than in the LG group but did not exceed 6 mitoses/10 HPF (Figure 1F); necrosis was absent.

All 12 cases classified as HG had a scarce stroma and were composed of hypercellular, largely overlapping cell population with a high nuclear to cytoplasmic ratio, hyperchromatic nuclei, and significant variability in cell shape. The cases were arranged in a herringbone pattern, vague fascicles, or solid sheets (Figure 2A,B). The mitotic activity ranged from 11 to 56 mitoses/10 HPF and small areas of necrosis were often present. In case 17, the tumor exhibited epithelioid to rhabdoid tumor cells (Figure 2C). Case 18 showed areas with unusual LG triphasic morphology resembling fibrous hamartoma of infancy (Figure 3A) that transformed into HG-IFS in some foci (Figure 3B) [20]. A typical LG-SPH pattern (Figure 3C) with progression to HG-IFS (Figure 3D) was present in case 6. Case 1 had the typical IFS morphology and contained a rich non-neoplastic inflammatory infiltrate (Figure 3E).

Immunohistochemical findings

The immunohistochemical results are summarized in Table 1. CD34 (Figures 3F,H and 4C) and S100 protein (Figures 3G,I and 4D) were at least focally positive in

© 2024 The Authors. *The Journal of Pathology* published by John Wiley & Sons Ltd on behalf of The Pathological Society of Great Britain and Ireland. www.pathsoc.org

10969896, 2024, 1, Downloaded from https://pathsocjournals.onlinelibrary.wiley.com/doi/10.1002/path.6260 by Ukraine - Cochrane, Wiley Online Library on [11/12/2024]. See the Terms and Conditions (https://onlinelibrary.wiley.com/terms-and-conditions) on Wiley Online Library for rules of use; OA articles are governed by the applicable Creative Commons License

Table 1. Main clinicopathological and molecular data.

Case No.	Age/sex	Localization	Max. dim. (cm)	Grade	Morphology review	Immunohistochemistry			Fusions detected by RNA-seq	Additional pathogenic mutations by DNA-seq	*CDKN2A* enumeration by FISH and/or methylation profiling	MSI/TMB (mut/Mb)	Methylation class by t-SNE clustering	Treatment	Outcome/length (months)
						S100	CD34	panTrk							
1	3 y/F	Lower eyelid	NA	HG	IFS	+	+++	+++	*LMNA::NTRK1*	–	Normal	NA/low	IMT	S + TT-E	2× LR before our diagnosis; NED/13
2	37 y/F	Instep	1.3	LG	LNT	+	+++	++	*LMNA::NTRK1*	–	Normal	NA	ND	S	NED/35
3	43 y/M	Hip	6.3	IG	SPH	++	+++	+++	*LMNA::NTRK1*	–	Loss†	Low/low	IFS	S	NED/10
4	1 d/M	Duodenum	NA	HG	IFS	–	–	+++	*TPM3::NTRK1*	–	Normal	NA	NA	CHT + TT-L	AWD/20
5	10 mo/M	Lower leg	NA	LG	LNT	+	–	+++	*TPM3::NTRK1*	NA	Normal	NA	ND	NA	NA
6*	3 y/M	Upper lip and orbit	NA	HG	IFS	+++	+++	+++	*EML4::NTRK3*	NA	Loss‡	Low/high (17.7)	IFS	S + CHT	Mediastinal MTS; DOD/30
				LG	SPH	++	+++	+++		NA	Normal	NA	ND		
7	4 mo/M	Forearm	NA	HG	IFS	–	–	++	*ETV6::NTRK3*	–	ND	Low/low	ND	S + CHT + TT-L	NED/27
8	5 mo/M	Cheek	NA	HG	IFS	–	+	+	*ETV6::NTRK3*	NA	ND	NA	ND	S + CHT	AWD/121
9	6 mo/F	Foot	NA	HG	IFS	–	++	++	*ETV6::NTRK3*	–	ND	NA	ND	CHT + TT-L	NED/21
10	1 mo/M	Scalp, intracranial propagation	4.7	HG	IFS	–	+	+++	*ETV6::NTRK3*	–	Normal	Low/low	ND	S	NA
11	26 y/F	Uterus	22.7	LG	Myxoid SPH with epithelioid/ rhabdoid cells	+++	+++	+++	*STRN::NTRK3*	–	Normal	NA	IFS	S	NA
12	13 y/F	Retroperitoneum	NA	LG	SPH	+	+++	+++	*RBPMS::NTRK3*	ND	ND	ND	ND	NA	LR; AWD/NA
13	14 d/F	Coccygeal region	1.5	HG	IFS	–	–	–	*PWWP2A::RET*	NA	Normal	NA	IFS	CHT + TT-S	AWD/22
14	10 mo/M	Nuchal region	4	IG	LG-MPNST-like	–	–	–	*CCDC6::RET*	NA	Normal	NA	ND	S	NA
15	6 y/F	Orbit	2	IG	SPH	++	+	–	*MYH10::RET*	–	Loss‡	Low/low	NA	S + CHT + TT-S	AWD/22
16	34 y/M	Forearm	NA	LG	LNT/SPH	+++	+++	–	*NCOA4::RET*	NA	NA	NA	ND	S (R1)	LR/48; later LFU
17	62 y/F	Thigh	13	HG	Epithelioid/ rhabdoid cells	–	–	ND	*NUMA1::RET*	ND	ND	ND	ND	NA	Recent case
18	1 d/F	Back	18	HG	Triphasic/IFS	++	+++	–	*TFG::MET*	*MYC* gain†	Normal	Low/high (35.4)	IFS	S	NED/130
19	72 y/F	Retroperitoneum	30	IG	MP	–	–	ND	*CAPZA2::MET*	NA	Loss†	NA	IFS	None	DU/NA
20	56 y/M	Knee	1.5	HG	IFS	–	+++	–	*ITSN1::RAF1*	–	ND	Low/low	ND	S	NED/10
21	5 mo/M	Retroperitoneum	5	HG	IFS	+++	–	–	*OSBP::BRAF*	–	Normal	NA	IFS	S + CHT	NED/29
22	46 y/F	Cervix	0.8	LG	SPH	+++	+++	–	–	*BRAF* delins; *EGFR* dup	Normal	NA	IFS	S	NA

*LG and HG areas present in two different blocks and analyzed separately.
†Confirmed by CNV analysis.
‡Homozygous loss confirmed by FISH.
+, 1–33% positive cells; ++, 34–66%; +++, 67–100%.
amp, amplification; AWD, alive with disease; CHT, chemotherapy; d, day; del, deletion; delins, deletion–insertion; dup, duplication; DOD, died of disease; DU, died, undetermined cause of death; HG, high grade; IFS, infantile fibrosarcoma pattern; IG, intermediate grade; ins, insertion; LFU, lost to follow-up; LG, low grade; LNT, lipofibromatosis-like neural tumor pattern; LR, local recurrence; m, months; MPNST, malignant peripheral nerve sheath tumor; MP, myopericytoma-like tumor pattern; MTS, metastasis; NA, not available; ND, not done; NED, no evidence of disease; pm, point mutation; SPH, pattern with stromal and perivascular hyalinization; S, surgery; TT-E, targeted therapy, entrectinib; TT-L, targeted therapy, larotrectinib; TT-S, targeted therapy, selpercatinib.

© 2024 The Authors. *The Journal of Pathology* published by John Wiley & Sons Ltd on behalf of The Pathological Society of Great Britain and Ireland. www.pathsoc.org

10969896, 2024, 1, Downloaded from https://pathsocjournals.onlinelibrary.wiley.com/doi/10.1002/path.6260 by Ukraine - Cochrane, Wiley Online Library on [11/12/2024]. See the Terms and Conditions (https://onlinelibrary.wiley.com/terms-and-conditions) on Wiley Online Library for rules of use; OA articles are governed by the applicable Creative Commons License

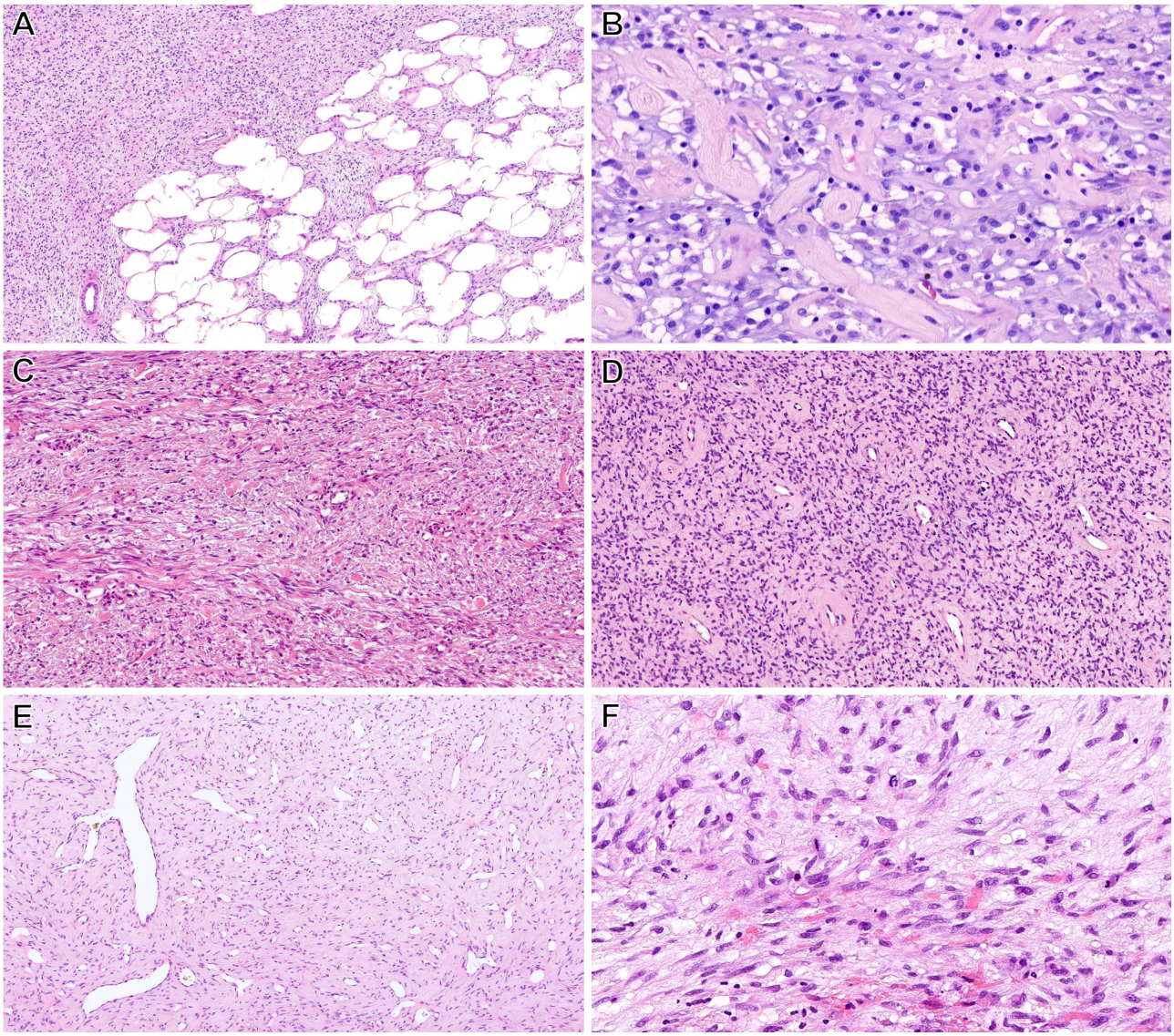


Figure 1. (A) Case 5 showed a prototypical LNT pattern with wide infiltration into subcutaneous adipose tissue. (B) Case 11 showed a myxoid SPH pattern composed mostly of epithelioid cells with abundant eosinophilic cytoplasm. (C and D) Cases 14 and 15 exhibited increased cellularity and were classified as IG. The former case had an LG-MPNST pattern (C), while the latter showed IG-SPH morphology (D). (E) Case 19 had a myopericytomatous pattern, and the tumor was composed of myoid spindle cells with low to moderate cellularity arranged in haphazard fascicles punctuated by abundant thin-walled vessels, some of which had a staghorn shape. Some areas had increased cellularity and mitotic activity (F).

14/22 (64%) and 12/22 (55%) cases, respectively, with both markers being expressed in 10/22 (45%) cases. All 12 cases with *NTRK* fusions were positive for panTrk (Figure 3J).

Molecular genetic findings

RNA and DNA sequencing

The main molecular-genetic results are presented in Table 1, and more detailed summaries are available in supplementary material, Tables S2 and S3.

NTRK1/3 fusions were revealed by RNA-seq in 12 cases, including four cases with IFS morphology and *ETV6::NTRK3* fusion. Case 6 with *EML4::NTRK3* was composed of LG-SPH areas transforming into IFS (Figure 3C,D). A uterine case with *STRN::NTRK3* showed an extraordinary, highly myxoid LG-SPH pattern (Figure 1B) [23], while case 12 with *RBPMS::NTRK3* fusion exhibited the LG-SPH pattern. The five *NTRK1*-fused tumors spanned the entire morphological spectrum, showing LG-LNT ($n = 2$), IG-SPH ($n = 1$), and HG-IFS ($n = 2$) patterns.

Tumors with *RET* fusions ($n = 5$) also spanned the entire spectrum from LG to HG lesions and showed various morphologies including the IFS pattern encountered in case 13 with a novel *PWWP2A::RET* fusion (Figure 2B). A novel *NUMA1::RET* fusion was detected in case 17 which showed epithelioid/rhabdoid morphology (Figure 2C). Both cases with *MET* fusion were unusual. Case 18 with *TFG::MET* fusion displayed a unique LG triphasic morphology (Figure 3A) combined with HG-IFS areas (Figure 3B) [20], while case 19 with

© 2024 The Authors. *The Journal of Pathology* published by John Wiley & Sons Ltd on behalf of The Pathological Society of Great Britain and Ireland. www.pathsoc.org

10969896, 2024, 1, Downloaded from https://pathsocjournals.onlinelibrary.wiley.com/doi/10.1002/path.6260 by Ukraine - Cochrane, Wiley Online Library on [11/12/2024]. See the Terms and Conditions (https://onlinelibrary.wiley.com/terms-and-conditions) on Wiley Online Library for rules of use; OA articles are governed by the applicable Creative Commons License

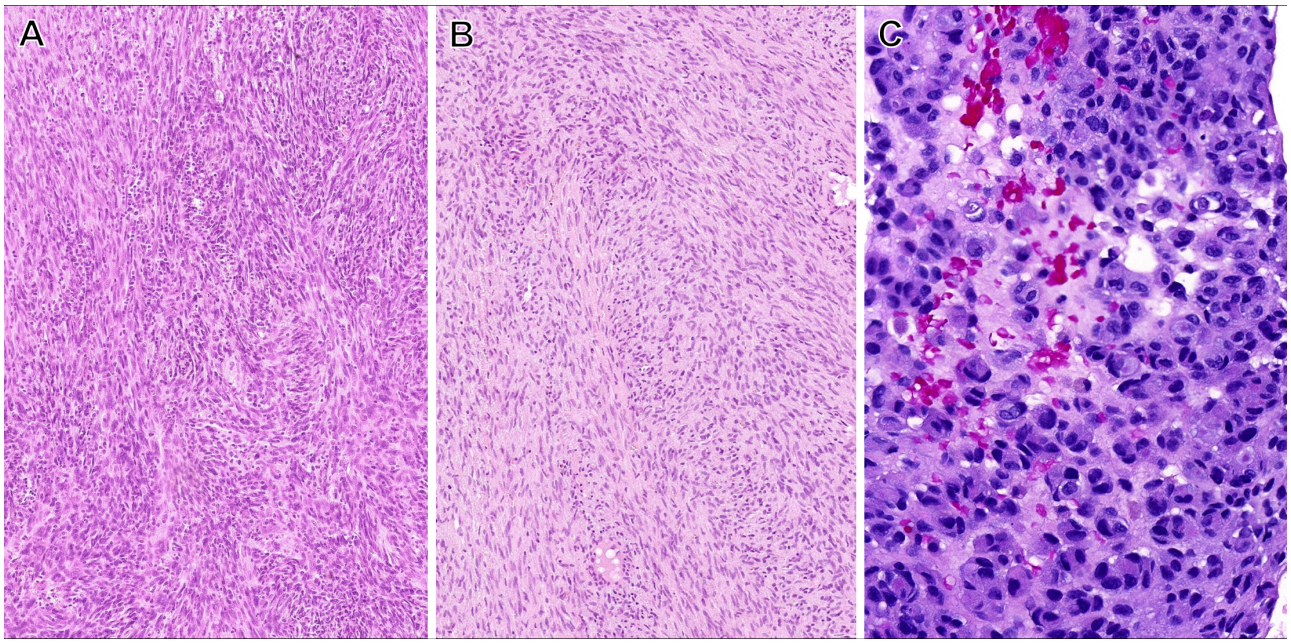


Figure 2. (A) Case 20 with a novel *ITSN1::RAF1* fusion and IFS morphology. (B) IFS morphology was also encountered in case 13, which harbored a novel *PWWP2A::RET* fusion. (C) Case 17 revealed epithelioid to rhabdoid tumor cells with HG atypia.

the *CAPZA2::MET* fusion had an IG myopericytomatous appearance (Figure 1E,F).

Both cases with *RAF1* ($n = 1$) and *BRAF* ($n = 1$) fusion showed IFS morphology (Figure 2A). Case 22 with an LG-SPH pattern (Figure 4A,B) lacked fusions but harbored a pathogenic *BRAF* delins p.V600K and an *EGFR* p.S768_D770dup.

DNA-seq was successful in 13 cases and uncovered rare additional genetic aberrations, mostly variants of unknown significance, with only two exceptions: likely pathogenic mutations of *PALB2* (case 11) and *ROS1* (case 18) of suspected and confirmed germline origin, respectively (supplementary material, Table S3). Additionally, in case 18, a CNV (duplication) of *MYC* was revealed by DNA-seq and confirmed by the methylation profiling CNV plot. A high TMB was detected in 2/8 tested cases (cases 6 and 18, 17.7 and 35.4 mut/Mb, respectively). All seven tested cases had low MSI.

Methylation profiling

Methylation profiling was successful in 9/11 cases. Case 13 with IFS morphology harboring the novel *PWWP2A::RET* fusion matched to the DKFZ sarcoma methylation class of infantile fibrosarcoma with a calibrated score of 0.98. No other match was found. However, in cases 3, 6, and 22, the classifier suggested a methylation class sarcoma, MPNST-like with low calibrated scores (0.73, 0.8, and 0.31, respectively). The other suggested methylation classes were DFSP for case 11 (score 0.57) and rhabdomyosarcoma-like in case 21 (score 0.43). No methylation class was suggested in three cases.

Unsupervised clustering of methylation profiles by t-SNE showed that the eight kinase-rearranged cases (cases 3, 6, 11, 13, 18, 19, 21, and 22) that passed quality control clustered together with the IFS methylation class and were distinct from 15 other soft tissue tumor types and control reactive tissue, including nerve sheath tumors, myofibroblastic tumors, and undifferentiated sarcomas (Figure 5A). Case 1, which contained a significant proportion of admixed inflammatory cells (Figure 3E), was the only case that clustered with IMT. This finding was further confirmed by hierarchical clustering. Figure 5B presents a heatmap showing the top 1,000 most variable CpG sites and similar methylation profiles between the eight kinase-rearranged tumors and the IFS methylation class, regardless of the underlying kinase fusion. Based on unsupervised hierarchical clustering, the MPNST-like methylation class showed the second most closely related methylation profile to the kinase-rearranged cases, while the MPNST methylation class showed a very distinct and different methylation signature.

Next, we analyzed and compared the percentages of genome-wide copy number alterations in the kinase-rearranged cases, comparing morphologically LG/IG with HG tumors. The HG cases (cases 6, 13, 18, 21) showed frequent copy number gains and losses, non-recurrently involving gains in *CCND1* (case 13), *MDM2/CDK4* (cases 6 and 18), and *CDK6* (case 21), and losses in *CDKN2A/B* (case 6) (Figure 6A), compared with the relatively flat copy number profile in LG cases (cases 3, 11, 19, 22) (Figure 6B). However, *CDKN2A/B* loss was also present in two LG cases (cases 3 and 19). Of note, the clinicopathological features of the two cases with *MDM2* gain were not in keeping with a diagnosis of dedifferentiated liposarcoma or intimal sarcoma with kinase gene fusions as recently reported [27]. Overall, the percentage of the genome involved by

© 2024 The Authors. *The Journal of Pathology* published by John Wiley & Sons Ltd on behalf of The Pathological Society of Great Britain and Ireland. www.pathsoc.org

10969896, 2024, 1, Downloaded from https://pathsocjournals.onlinelibrary.wiley.com/doi/10.1002/path.6260 by Ukraine - Cochrane, Wiley Online Library on [11/12/2024]. See the Terms and Conditions (https://onlinelibrary.wiley.com/terms-and-conditions) on Wiley Online Library for rules of use; OA articles are governed by the applicable Creative Commons License

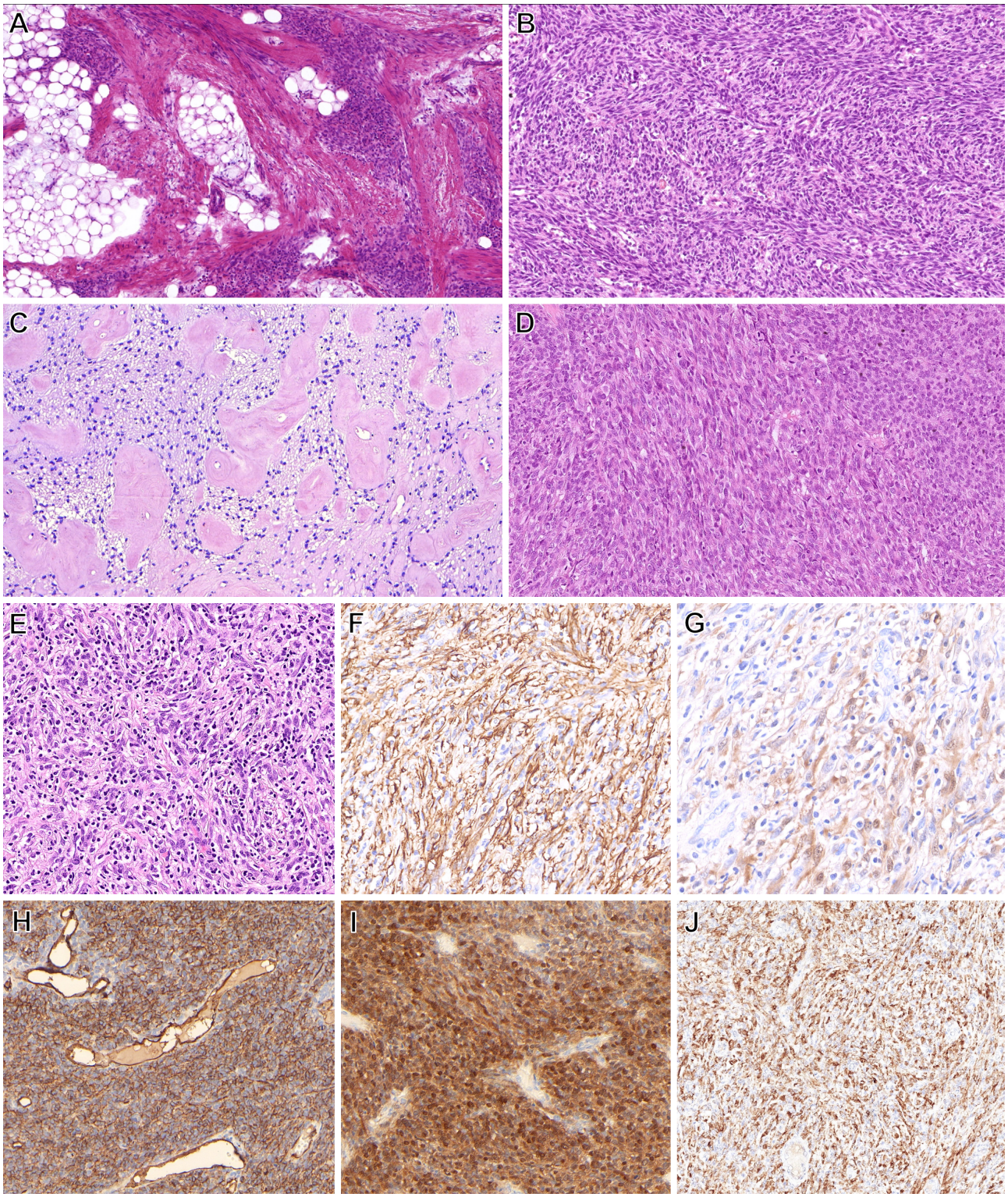


Figure 3. (A) Case 18 showed areas with unusual LG triphasic morphology resembling fibrous hamartoma of infancy, which in some areas transformed into IFS areas (B). (C and D) Case 6 with *EML4::NTRK3* was composed of LG-SPH areas (C) transforming into an HG-IFS morphology (D). (E) Case 1 with *LMNA::NTRK1* contained a significant inflammatory infiltrate and clustered with the IMT methylation class. Both CD34 (F) and S100 (G) were positive. (H and I) The tumor in case 6 co-expressed both CD34 (H) and S100 protein (I). In addition, diffuse panTrk expression was present (J).

CNVs, serving as a surrogate for genomic complexity, in HG cases was significantly higher than those in LG–IG tumors (mean % CNV: 24.7% versus 7.0%, Student-*t* $p < 0.036$) (Figure 6C).

FISH

In addition, the loss of the *CDKN2A* gene locus was analyzed using FISH, confirming homozygous loss in cases 6 and 15. In case 6, loss of *CDKN2A* was present

© 2024 The Authors. *The Journal of Pathology* published by John Wiley & Sons Ltd on behalf of The Pathological Society of Great Britain and Ireland. www.pathsoc.org

10969896, 2024, 1, Downloaded from https://pathsocjournals.onlinelibrary.wiley.com/doi/10.1002/path.6260 by Ukraine - Cochrane, Wiley Online Library on [11/12/2024]. See the Terms and Conditions (https://onlinelibrary.wiley.com/terms-and-conditions) on Wiley Online Library for rules of use; OA articles are governed by the applicable Creative Commons License

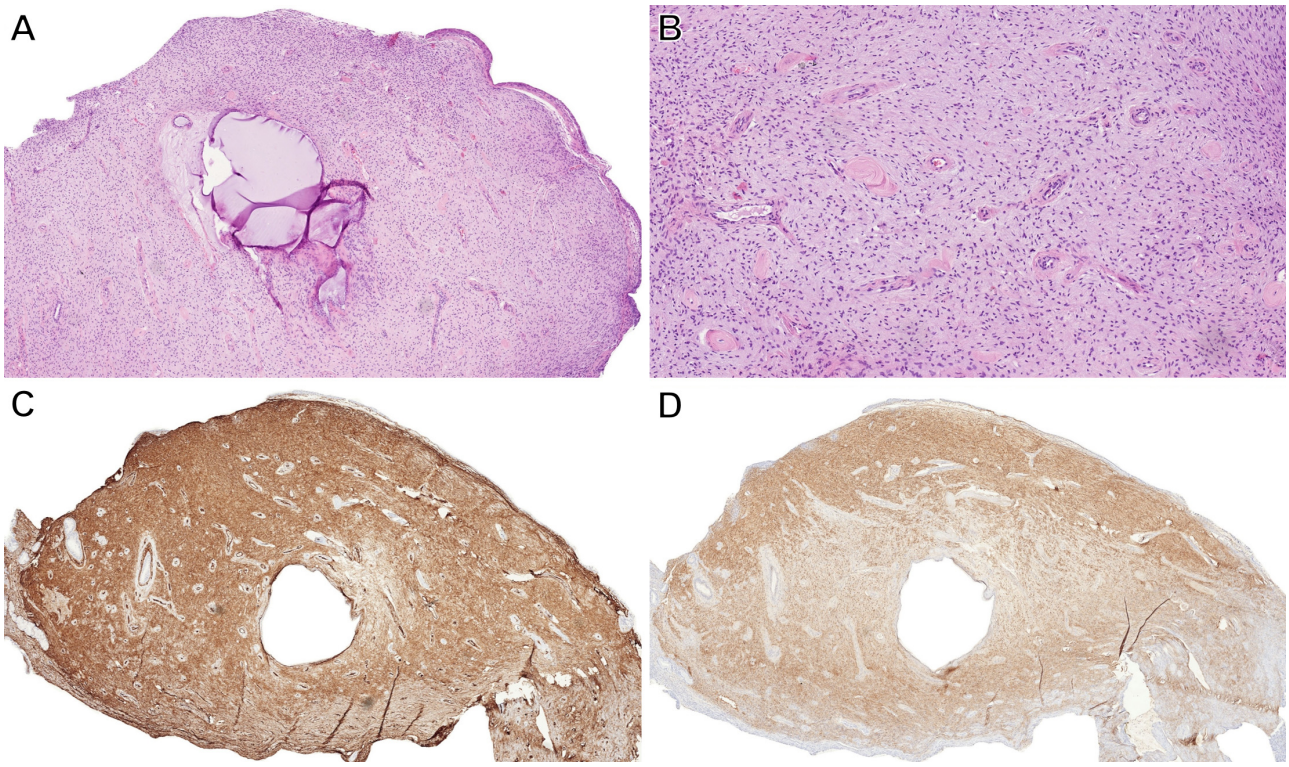


Figure 4. (A–D) No fusion was found in case 22 with an LG-SPH pattern (A and B), which instead harbored a pathogenic *BRAF* delins p.V600K and a pathogenic in-frame duplication in *EGFR* p.S768_D770dup. The tumor co-expressed CD34 (C) and S100 protein (D).

only in the IFS-like component (independently confirmed by a CNV plot), while the LG-SPH areas analyzed separately by FISH had both copies intact.

Treatment and follow-up data

Treatment and follow-up data as summarized in Table 1 were available for 19 and 16 patients, respectively. Follow-up length ranged from 10 to 130 months (mean 38 months; median 24.5 months). Overall, the recurrence and metastatic rates in our study were 19% and 6%, respectively. The only tumor that metastasized and eventually had a fatal outcome (case 6) showed HG-IFS morphology. In case 19, the patient had a large inoperable retroperitoneal tumor and died of an unknown cause.

In 12/19 cases, including eight cases with follow-up data, the patients were treated by surgery with ($n = 3$) or without ($n = 9$) chemotherapy. The status of surgical margins was mostly unknown. Overall, five patients had no evidence of disease (NED) with follow-up length ranging from 10 to 130 months; one case recurred 48 months after an R1 excision; and one patient was alive with disease (AWD). The patient in case 6 experienced distant metastasis and eventually died of the tumor in 30 months.

Six patients were treated with targeted therapy combined with surgery and/or chemotherapy. The eyelid tumor in case 1 had repeatedly recurred before being diagnosed as an *NTRK1*-rearranged tumor. The patient was then started on entrectinib and 13 months later had NED. In case 7, the incompletely excised tumor was further treated with chemotherapy and larotrectinib, leading to complete response (NED, 27 months). The patient in case 15 was initially treated with surgery and chemotherapy. Selpercatinib was then administered, leading to significant regression of the residual tumor within 2 months (AWD, 22 months). Complete response with chemotherapy and larotrectinib was achieved in case 9 (NED, 21 months). Minimal response to chemotherapy but almost complete response to selpercatinib was observed in case 13 (minimal residual tumor, 22 months). Larotrectinib was discontinued due to severe side effects in case 4 (AWD, 20 months).

Discussion

The distinction between IFS and *NTRK*-SCN as currently defined by the WHO is mostly straightforward as they usually occur at different ages. However, due to a significant overlap in diagnostic criteria, a subset of cases could be assigned to both groups, particularly infantile cases with alternative kinase fusions and IFS morphology that co-express CD34 and/or S100 protein. In fact, some studies speculated that all pediatric *NTRK*-rearranged mesenchymal tumors including IFS may represent a single disease [13]. While the inability for precise classification does not currently affect the patients' management, gaining this ability might eventually prove to be of prognostic or therapeutic relevance.

© 2024 The Authors. *The Journal of Pathology* published by John Wiley & Sons Ltd on behalf of The Pathological Society of Great Britain and Ireland. www.pathsoc.org

10969896, 2024, 1, Downloaded from https://pathsocjournals.onlinelibrary.wiley.com/doi/10.1002/path.6260 by Ukraine - Cochrane, Wiley Online Library on [11/12/2024]. See the Terms and Conditions (https://onlinelibrary.wiley.com/terms-and-conditions) on Wiley Online Library for rules of use; OA articles are governed by the applicable Creative Commons License

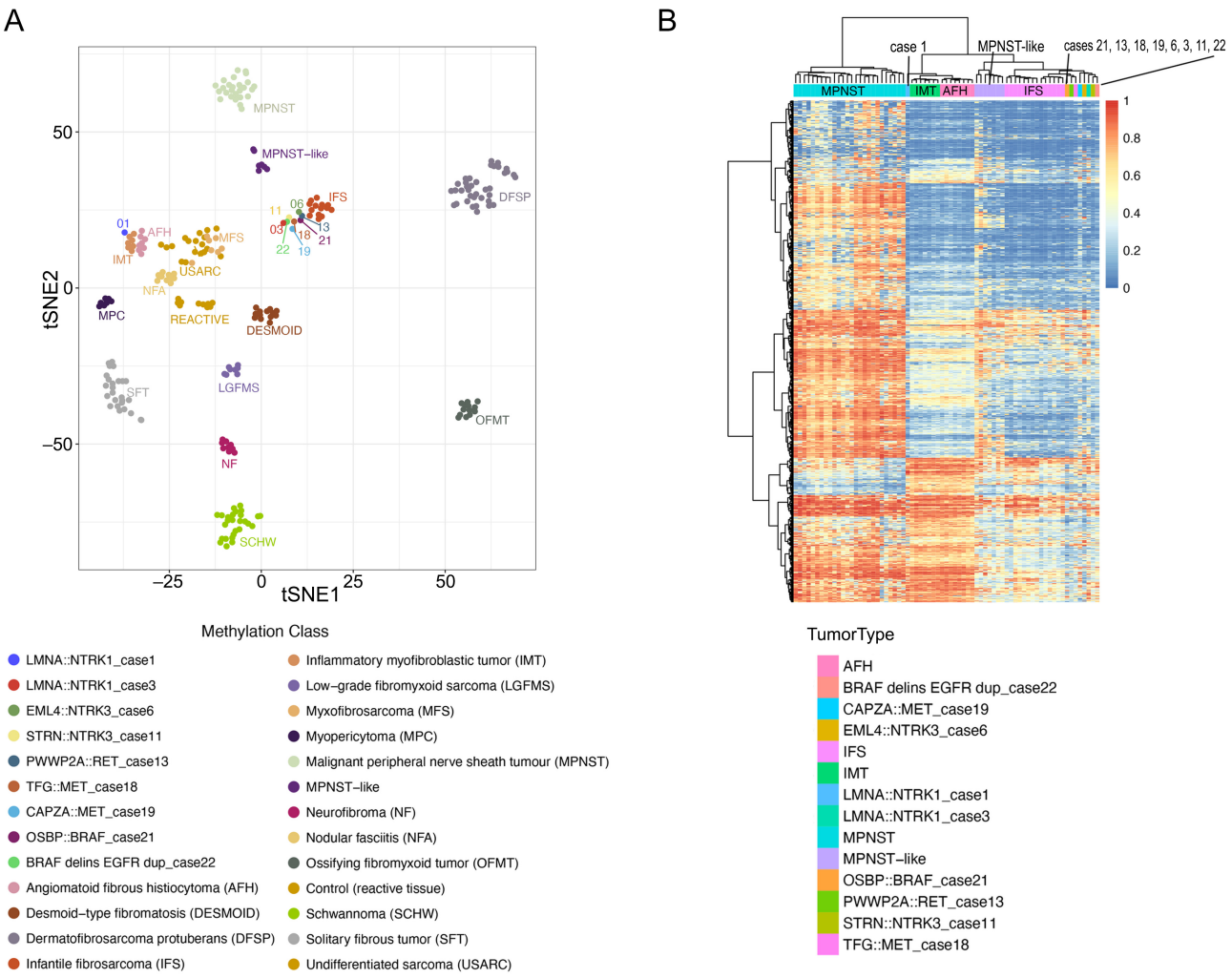


Figure 5. (A) Unsupervised clustering of methylation profiles by t-SNE compared with 247 miscellaneous soft tissue methylation classes showed that eight cases (cases 3, 6, 11, 13, 18, 19, 21, and 22) clustered together with the IFS methylation class and one case (case 1) clustered with IMT. (B) Unsupervised hierarchical clustering of methylation profiles comparing these nine cases of kinase-rearranged tumors with IFS, IMT, MPNST, and MPNST-like cases demonstrated similar findings.

Given the relatively short median follow-up and multiple factors influencing prognosis (margin status, selected therapy, etc.), of which some are unknown in our study, any comparison of clinical behavior between *NTRK*-SCN and IFS would be inaccurate based on our data. However, the only case in our study that metastasized and eventually led to the patient's death was case 6 with HG morphology, which supports the previously mentioned assumption [9] that at least in adult patients [1] the metastatic potential of *NTRK*-SCN seems to partially correlate with histologic grade, as tumors with low cellularity, atypia, and mitotic activity generally tend to follow an indolent clinical course [14,28]. However, rare exceptions may occur [29]. From the therapeutic perspective, our study further confirms the effectiveness of targeted therapy with *NTRK* and *RET* inhibitors [30,31], leading to a complete or near-complete response in 5/6 cases.

Very interesting novel data regarding the relationship between *NTRK*-SCN and IFS were recently published by Tauziède-Espariat *et al* [29]. Using unsupervised whole RNA-seq clustering analysis, they showed that almost all infantile and adult cases with *NTRK* fusions (and one *MET*-rearranged case) including *ETV6::NTRK3*-fused IFS cluster closely together independently of their clinicopathological features. Moreover, using DNA methylation-based DKFZ brain tumor and sarcoma classifiers [25,26], 9/16 cases were significantly classified (calibrated scores ≥ 0.9) either as sarcoma, MPNST-like ($n = 6$) or as IFS ($n = 3$). Then, on t-SNE analysis of the methylation data, their cohort segregated into three different subgroups. While four tumors (4/16, 25%) occurring in infants aged 0–1 year, with IFS morphology, CD34 and S100-negative immunoprofile, and *ETV6::NTRK3* fusion classified within the IFS cluster, the largest fraction (11/16, 69%) formed a possibly novel cluster very close to the existing methylation class sarcoma, MPNST-like. Six out of the 11 cases (54.5%) had a *CDKN2A* deletion, an aberration not found in other tumors in the study. This methylation cluster included tumors irrespective of age that were initially diagnosed by histopathology either as *NTRK*-SCN or as adult-type

© 2024 The Authors. *The Journal of Pathology* published by John Wiley & Sons Ltd on behalf of The Pathological Society of Great Britain and Ireland. www.pathsoc.org

10969896, 2024, 1, Downloaded from https://pathsocjournals.onlinelibrary.wiley.com/doi/10.1002/path.6260 by Ukraine - Cochrane, Wiley Online Library on [11/12/2024]. See the Terms and Conditions (https://onlinelibrary.wiley.com/terms-and-conditions) on Wiley Online Library for rules of use; OA articles are governed by the applicable Creative Commons License

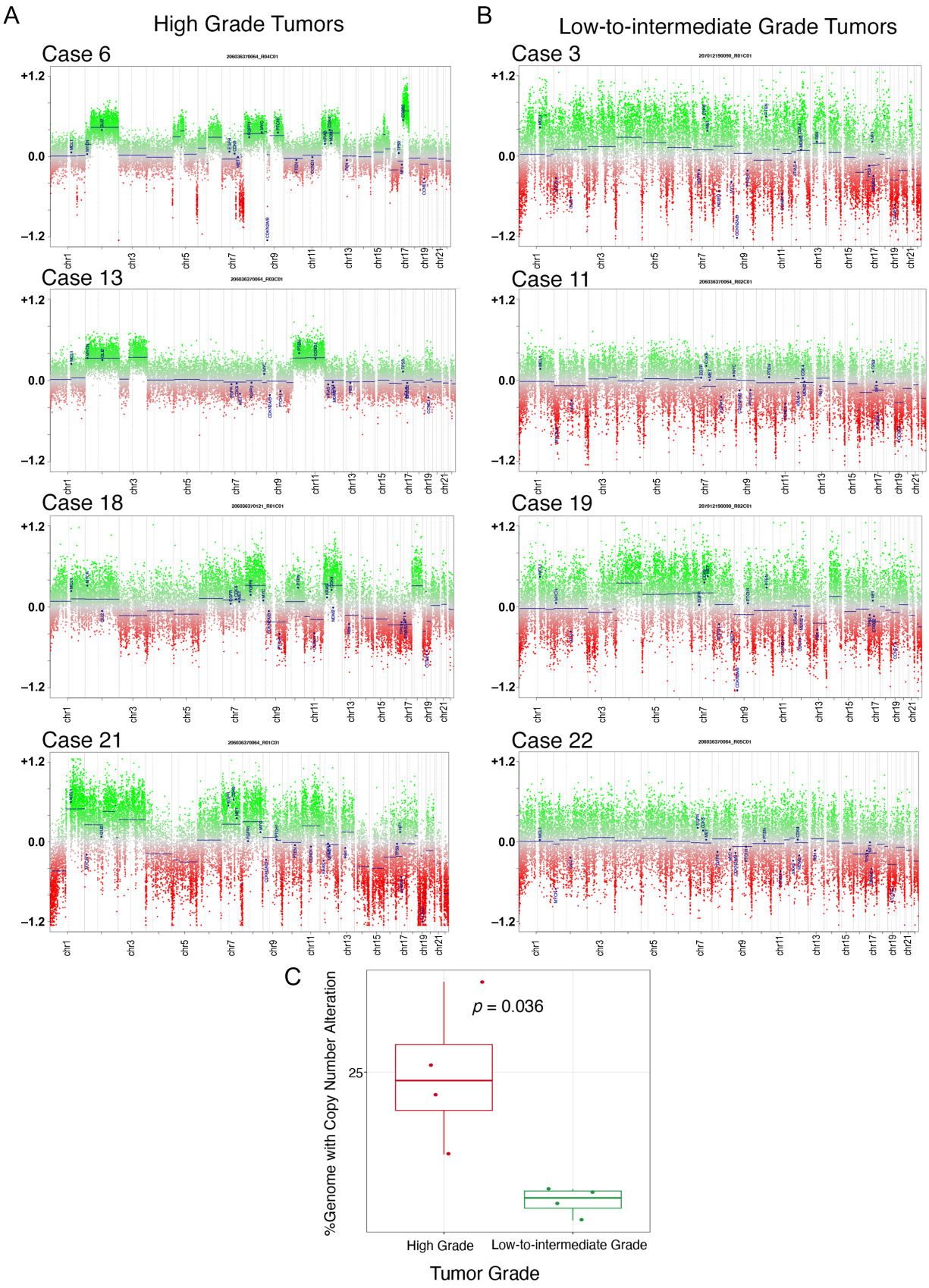


Figure 6. Percentage of genome CNAs in low to intermediate- and high-grade cases. Genome-wide CNA obtained from the methylation profile using the conumee R package. (A and B) Copy number profiles of high-grade (A) and low to intermediate-grade cases (B) across the genome with copy number segments computed over genomic regions with gains or losses. Each dot represents a CpG probe. (C) Copy number alterations: the center line corresponds to the median; lower and upper hinges correspond to the 25th and 75th percentiles; upper and lower whiskers correspond to 1.5 × interquartile range. Each dot represents an individual case. *p* value from Student's *t*-analysis.

© 2024 The Authors. *The Journal of Pathology* published by John Wiley & Sons Ltd on behalf of The Pathological Society of Great Britain and Ireland. www.pathsoc.org

10969896, 2024, 1, Downloaded from https://pathsocjournals.onlinelibrary.wiley.com/doi/10.1002/path.6260 by Ukraine - Cochrane, Wiley Online Library on [11/12/2024]. See the Terms and Conditions (https://onlinelibrary.wiley.com/terms-and-conditions) on Wiley Online Library for rules of use; OA articles are governed by the applicable Creative Commons License

fibrosarcomas; all showed CD34 and S100 co-expression, and all had either *NTRK* or *MET* fusions [29].

In contrast to these findings [29], our results show that irrespective of their clinical, morphological, or genetic features, the methylation profiles of the eight kinase-rearranged cases clustered together with the IFS methylation class, while being distinct from 15 other soft tissue tumor types (including the MPNST-like group) and control reactive tissue. This finding was further confirmed by hierarchical clustering. Interestingly, the MPNST-like methylation class represented the second most closely related methylation profile, while the MPNST methylation class showed a very distinct and different methylation signature. Notably, case 1 with a rich inflammatory background clustered together with the IMT methylation class, a common phenomenon observed in tumors with abundant inflammatory cells. The disagreement between the two studies is difficult to explain but might be caused by differences in study cohorts or different methylation classes being included in the unsupervised clustering analysis. Nevertheless, it is important to note that the MPNST-like methylation class is currently not very well characterized and is supposed to include cases with MPNST-like morphology, retained expression of the H3K27 trimethylation marker, and a high frequency of *CDKN2A/B* homozygous deletions [26]. Therefore, this group may include a heterogeneous mixture of tumors, including some with kinase fusions, possibly explaining the close relationship of cases in our study as well as in the study by Tauziède-Espariat *et al* [29]. More studies are still needed to elucidate the exact link between *NTRK*-SCN and IFS.

On the other hand, when we attempted tumor classification using the DKFZ sarcoma methylation classifier, only the congenital case 13 with *PWWP2A::RET* fusion significantly classified (score 0.98) with the methylation class IFS. To the best of our knowledge, this is the first reported case assigned to this methylation class within this classifier that harbors a fusion different from *ETV6::NTRK3*. An additional three cases were assigned to the methylation class sarcoma, MPNST-like, but with low calibrated scores. Such inconsistent and highly variable results likely reflect the fact that the original training and validation cohort in the sarcoma classifier lacked a well-characterized cohort of *NTRK*-SCN, and thus is inadequate in this tumor class.

CNV plots were generated in all cases where methylation profiling was possible. This allowed us to correlate the CNV profiles of each case with their morphological features. Our results indicate a relatively good concordance between a flat CNV profile and LG/IG morphology. In contrast, multiple gains and losses were usually found in HG cases. Specifically, about 25% of the genome in the HG group was involved by non-recurrent copy number gains and losses, compared with only 7% in the LG and IG group. *CDKN2A/B* loss is a non-recurrent feature of tumors in the latter group, which was also shown in the study by Tauziède-Espariat *et al* [29]. Additionally, we also observed non-recurrent copy number gains in *CDKNA2A/B*, *CCND1*, *MDM2/CDK4*, and *CDK6* among our HG cases. Short follow-up data for most of our cases hindered a reliable comparison of CNV profiles with prognosis but the only case with a fatal outcome (case 6) had a highly complex CNV profile, which is in keeping with a previous study on this topic [32].

Our study also presented four gene fusions that are novel in soft tissue tumors, namely *PWWP2A::RET*, *NUMA1::RET*, *CAPZA2::MET*, and *ITSN1::RAF1*. The *PWWP2A* gene, which encodes a protein involved in histone acetylation [33], was previously identified as a fusion partner to *ROS1* in Spitz tumors [34,35]. *NUMA1* fusions, whose product, NuMA, plays an important role in mitotic spindle assembly and function [36], were reported in acute promyelocytic leukemia [37], as well as in rare cases of IMT [38] and aneurysmal fibrous histiocytoma [39]. *CAPZA2*, encoding an actin-binding protein, CapZ [40], was previously detected as a *MET* fusion partner in non-small cell lung cancer [41]. To the best of our knowledge, no fusions or other alterations of the *ITSN1* gene (encoding a vesicle scaffolding protein, intersectin-1 [42]) have been reported to date. Overall, the pathogenic effects of all these novel fusions most likely derive from the fusion partner containing the tyrosine or serine/threonine kinase domain, i.e. *NTRK1/3*, *RET*, *RAF1*, or *MET*. Proteins encoded by these genes are all part of the ubiquitous MAP kinase signaling cascade, and the general mechanism by which they lead to oncogenesis has been thoroughly described [1,34]. Of these four novel fusions, the most interesting is *CAPZA2::MET* as only five *MET*-rearranged mesenchymal tumors have been described in the literature [5,9,20,35]. Our case is distinct from them both morphologically and clinically since it is the first such case reported in an adult.

This study also included two uterine cases. While the first harbored an *NTRK3* fusion [23], which is well known to occur in uterine mesenchymal tumors [43–45], the latter (case 22) was extraordinary. It had the typical morphology and immunoprofile of *NTRK*-SCN but instead of a fusion, it harbored pathogenic aberrations of *BRAF* and *EGFR*, which has not been seen previously in this context. However, *BRAF* as well as *EGFR* aberrations were recently reported in congenital mesoblastic nephroma, i.e. a tumor with a significant morphologic overlap with IFS and *NTRK*-SCN [21,22,46,47].

Despite rapidly increasing knowledge regarding the various driving molecular aberrations detected in kinase fusion mesenchymal tumors, larger-scale studies analyzing other potential molecular aberrations that could be responsible for therapy resistance or tumor progression were missing [48]. We used a large DNA panel to analyze 13 cases and found only rare secondary genetic aberrations with unclear significance.

In summary, we report a comprehensive clinicopathological and molecular genetic analysis of 22 cases of both pediatric and adult mesenchymal tumors with kinase gene aberrations. We detected four novel fusions not previously reported in these neoplasms, including

© 2024 The Authors. *The Journal of Pathology* published by John Wiley & Sons Ltd on behalf of The Pathological Society of Great Britain and Ireland. www.pathsoc.org

10969896, 2024, 1, Downloaded from https://pathsocjournals.onlinelibrary.wiley.com/doi/10.1002/path.6260 by Ukraine - Cochrane, Wiley Online Library on [11/12/2024]. See the Terms and Conditions (https://onlinelibrary.wiley.com/terms-and-conditions) on Wiley Online Library for rules of use; OA articles are governed by the applicable Creative Commons License

the first adult *MET*-rearranged case, as well as the first uterine case of this type lacking a fusion but harboring *BRAF* and *EGFR* mutations. In the methylation profiling analysis, 8/9 of our cases clustered together with the IFS methylation class, suggesting that they represent a closely related entity.

Acknowledgements

This study was supported by study grant SVV 260652 from the Ministry of Education, Czech Republic (NK, EM, AK, OK) and by the Cooperatio program, Research Area SURG (NK, Michael M).

Author contributions statement

All authors contributed to the study conception and edited the manuscript. Material preparation, final data collection and analysis were performed by NK and Michael M. JKD performed the methylation and CNV analysis. The first draft of the manuscript was written by NK, with a significant contribution from Michael M. All authors commented on previous versions of the manuscript. All authors read and approved the final manuscript.

Data availability statement

Data supporting the findings of this study are available within the article. The complete datasets generated during and/or analyzed during the current study are available from the corresponding author upon reasonable request.

References

1. Davis JL, Al-Ibraheemi A, Rudzinski ER, *et al*. Mesenchymal neoplasms with NTRK and other kinase gene alterations. *Histopathology* 2022; **80:** 4–18.
2. Knezevich SR, Garnett MJ, Pysher TJ, *et al*. *ETV6-NTRK3* gene fusions and trisomy 11 establish a histogenetic link between mesoblastic nephroma and congenital fibrosarcoma. *Cancer Res* 1998; **58:** 5046–5048.
3. Rubin BP, Chen CJ, Morgan TW, *et al*. Congenital mesoblastic nephroma t(12;15) is associated with *ETV6-NTRK3* gene fusion: cytogenetic and molecular relationship to congenital (infantile) fibrosarcoma. *Am J Pathol* 1998; **153:** 1451–1458.
4. Kao YC, Fletcher CDM, Alaggio R, *et al*. Recurrent *BRAF* gene fusions in a subset of pediatric spindle cell sarcomas – expanding the genetic spectrum of tumors with overlapping features with infantile fibrosarcoma. *Am J Surg Pathol* 2018; **42:** 28–38.
5. Flucke U, van Noesel MM, Wijnen M, *et al*. *TFG-MET* fusion in an infantile spindle cell sarcoma with neural features. *Genes Chromosomes Cancer* 2017; **56:** 663–667.
6. Church AJ, Calicchio ML, Nardi V, *et al*. Recurrent *EML4–NTRK3* fusions in infantile fibrosarcoma and congenital mesoblastic nephroma suggest a revised testing strategy. *Mod Pathol* 2018; **31:** 463–473.
7. Tan SY, Al-Ibraheemi A, Ahrens WA, *et al*. *ALK* rearrangements in infantile fibrosarcoma-like spindle cell tumours of soft tissue and kidney. *Histopathology* 2022; **80:** 698–707.
8. Kallen ME, Hornick JL. The 2020 WHO classification: what's new in soft tissue tumor pathology? *Am J Surg Pathol* 2021; **45:** e1–e23.
9. Antonescu CR. Emerging soft tissue tumors with kinase fusions: an overview of the recent literature with an emphasis on diagnostic criteria. *Genes Chromosomes Cancer* 2020; **59:** 437–444.
10. Agaram NP, Zhang L, Sung YS, *et al*. Recurrent *NTRK1* gene fusions define a novel subset of locally aggressive lipofibromatosis-like neural tumors. *Am J Surg Pathol* 2016; **40:** 1407–1416.
11. Suurmeijer AJH, Kao YC, Antonescu CR. New advances in the molecular classification of pediatric mesenchymal tumors. *Genes Chromosomes Cancer* 2019; **58:** 100–110.
12. Haller F, Knopf J, Ackermann A, *et al*. Paediatric and adult soft tissue sarcomas with *NTRK1* gene fusions: a subset of spindle cell sarcomas unified by a prominent myopericytic/haemangiopericytic pattern. *J Pathol* 2016; **238:** 700–710.
13. Davis JL, Lockwood CM, Stohr B, *et al*. Expanding the spectrum of pediatric *NTRK*-rearranged mesenchymal tumors. *Am J Surg Pathol* 2019; **43:** 435–445.
14. Suurmeijer AJH, Dickson BC, Swanson D, *et al*. A novel group of spindle cell tumors defined by S100 and CD34 co-expression shows recurrent fusions involving RAF1, BRAF, and NTRK1/2 genes. *Genes Chromosomes Cancer* 2018; **57:** 611–621.
15. Antonescu CR, Dickson BC, Swanson D, *et al*. Spindle cell tumors with RET gene fusions exhibit a morphologic spectrum akin to tumors with NTRK gene fusions. *Am J Surg Pathol* 2019; **43:** 1384–1391.
16. Davis JL, Vargas SO, Rudzinski ER, *et al*. Recurrent *RET* gene fusions in paediatric spindle mesenchymal neoplasms. *Histopathology* 2020; **76:** 1032–1041.
17. Dermawan JK, Azzato EM, Goldblum JR, *et al*. Superficial *ALK*-rearranged myxoid spindle cell neoplasm: a cutaneous soft tissue tumor with distinctive morphology and immunophenotypic profile. *Mod Pathol* 2021; **34:** 1710–1718.
18. Choo F, Rakheja D, Davis LE, *et al*. *GAB1-ABL1* fusions in tumors that have histologic overlap with *NTRK*-rearranged spindle cell tumors. *Genes Chromosomes Cancer* 2021; **60:** 623–630.
19. Michal M, Ptáková N, Martínek P, *et al*. S100 and CD34 positive spindle cell tumor with prominent perivascular hyalinization and a novel NCOA4-RET fusion. *Genes Chromosomes Cancer* 2019; **58:** 680–685.
20. Michal M, Ud Din N, Švajdler M, *et al*. *TFG::MET*-rearranged soft tissue tumor: a rare infantile neoplasm with a distinct low-grade triphasic morphology. *Genes Chromosomes Cancer* 2022; **62:** 290–296.
21. Penning AJ, Al-Ibraheemi A, Michal M, *et al*. Novel *BRAF* gene fusions and activating point mutations in spindle cell sarcomas with histologic overlap with infantile fibrosarcoma. *Mod Pathol* 2021; **34:** 1530–1540.
22. Wegert J, Vokuhl C, Collord G, *et al*. Recurrent intragenic rearrangements of *EGFR* and *BRAF* in soft tissue tumors of infants. *Nat Commun* 2018; **9:** 2378.
23. Michal M, Hájková V, Skálová A, *et al*. *STRN-NTRK3*-rearranged mesenchymal tumor of the uterus: expanding the morphologic spectrum of tumors with *NTRK* fusions. *Am J Surg Pathol* 2019; **43:** 1152–1154.
24. Gerami P, Li G, Pouryazdanparast P, *et al*. A highly specific and discriminatory FISH assay for distinguishing between benign and malignant melanocytic neoplasms. *Am J Surg Pathol* 2012; **36:** 808–817.
25. Capper D, Jones DTW, Sill M, *et al*. DNA methylation-based classification of central nervous system tumours. *Nature* 2018; **555:** 469–474.

© 2024 The Authors. *The Journal of Pathology* published by John Wiley & Sons Ltd on behalf of The Pathological Society of Great Britain and Ireland. www.pathsoc.org

10969896, 2024, 1, Downloaded from https://pathsocjournals.onlinelibrary.wiley.com/doi/10.1002/path.6260 by Ukraine - Cochrane, Wiley Online Library on [11/12/2024]. See the Terms and Conditions (https://onlinelibrary.wiley.com/terms-and-conditions) on Wiley Online Library for rules of use; OA articles are governed by the applicable Creative Commons License

26. Koelsche C, Schrimpf D, Stichel D, *et al*. Sarcoma classification by DNA methylation profiling. *Nat Commun* 2021; **12:** 498.
27. Brahmi M, Dufresne A, Verret B, *et al*. NTRK fusion in soft tissue sarcomas harboring MDM2/CDK4 amplification: three case reports. *Ann Oncol* 2021; **32:** 813–814.
28. Kao YC, Suurmeijer AJH, Argani P, *et al*. Soft tissue tumors characterized by a wide spectrum of kinase fusions share a lipofibromatosis-like neural tumor pattern. *Genes Chromosomes Cancer* 2020; **59:** 575–583.
29. Tauziède-Espariat A, Duchesne M, Baud J, *et al*. *NTRK*-rearranged spindle cell neoplasms are ubiquitous tumours of myofibroblastic lineage with a distinct methylation class. *Histopathology* 2022; **82:** 596–607.
30. Ortiz MV, Gerdemann U, Raju SG, *et al*. Activity of the highly specific RET inhibitor selpercatinib (LOXO-292) in pediatric patients with tumors harboring *RET* gene alterations. *JCO Precis Oncol* 2020; **4:** PO.19.00401.
31. Laetsch TW, DuBois SG, Mascarenhas L, *et al*. Larotrectinib for paediatric solid tumours harbouring NTRK gene fusions: phase 1 results from a multicentre, open-label, phase 1/2 study. *Lancet Oncol* 2018; **19:** 705–714.
32. Vargas AC, Ardakani NM, Wong DD, *et al*. Chromosomal imbalances detected in *NTRK*-rearranged sarcomas by the use of comparative genomic hybridisation. *Histopathology* 2021; **78:** 932–942.
33. Link S, Spitzer RMM, Sana M, *et al*. PWWP2A binds distinct chromatin moieties and interacts with an MTA1-specific core NuRD complex. *Nat Commun* 2018; **9:** 4300.
34. Donati M, Kastnerova L, Martinek P, *et al*. Spitz tumors with *ROS1* fusions: a clinicopathological study of 6 cases, including FISH for chromosomal copy number alterations and mutation analysis using next-generation sequencing. *Am J Dermatopathol* 2020; **42:** 92–102.
35. Wiesner T, He J, Yelensky R, *et al*. Kinase fusions are frequent in Spitz tumours and spitzoid melanomas. *Nat Commun* 2014; **5:** 3116.
36. Chu X, Chen X, Wan Q, *et al*. Nuclear mitotic apparatus (NuMA) interacts with and regulates astrin at the mitotic spindle. *J Biol Chem* 2016; **291:** 20055–20067.
37. Wells RA, Catzavelos C, Kamel-Reid S. Fusion of retinoic acid receptor alpha to NuMA, the nuclear mitotic apparatus protein, by a variant translocation in acute promyelocytic leukaemia. *Nat Genet* 1997; **17:** 109–113.
38. Rao N, Iwenofu H, Tang B, *et al*. Inflammatory myofibroblastic tumor driven by novel *NUMA1-ALK* fusion responds to ALK inhibition. *J Natl Compr Canc Netw* 2018; **16:** 115–121.
39. Panagopoulos I, Gorunova L, Bjerkehagen B, *et al*. *LAMTOR1-PRKCD* and *NUMA1-SFMBT1* fusion genes identified by RNA sequencing in aneurysmal benign fibrous histiocytoma with t(3;11)(p21;q13). *Cancer Genet* 2015; **208:** 545–551.
40. dos Remedios CG, Chhabra D, Kekic M, *et al*. Actin binding proteins: regulation of cytoskeletal microfilaments. *Physiol Rev* 2003; **83:** 433–473.
41. Riedel R, Fassunke J, Scheel AH, *et al*. *MET* fusions in NSCLC: clinicopathologic features and response to MET inhibition. *J Thorac Oncol* 2023; **19:** 160–165.
42. Herrero-Garcia E, O'Bryan JP. Intersectin scaffold proteins and their role in cell signaling and endocytosis. *Biochim Biophys Acta Mol Cell Res* 2017; **1864:** 23–30.
43. Chiang S, Cotzia P, Hyman DM, *et al*. *NTRK* fusions define a novel uterine sarcoma subtype with features of fibrosarcoma. *Am J Surg Pathol* 2018; **42:** 791–798.
44. Croce S, Hostein I, Longacre TA, *et al*. Uterine and vaginal sarcomas resembling fibrosarcoma: a clinicopathological and molecular analysis of 13 cases showing common *NTRK*-rearrangements and the description of a *COL1A1-PDGFB* fusion novel to uterine neoplasms. *Mod Pathol* 2019; **32:** 1008–1022.
45. Costigan DC, Nucci MR, Dickson BC, *et al*. *NTRK*-rearranged uterine sarcomas: clinicopathologic features of 15 cases, literature review, and risk stratification. *Am J Surg Pathol* 2022; **46:** 1415–1429.
46. Zhao M, Yin M, Kuick CH, *et al*. Congenital mesoblastic nephroma is characterised by kinase mutations including *EGFR* internal tandem duplications, the *ETV6-NTRK3* fusion, and the rare *KLHL7-BRAF* fusion. *Histopathology* 2020; **77:** 611–621.
47. Koo SC, Schieffer KM, Lee K, *et al*. *EGFR* internal tandem duplications in fusion-negative congenital and neonatal spindle cell tumors. *Genes Chromosomes Cancer* 2023; **62:** 17–26.
48. Thorwarth A, Haase K, Roefzaad C, *et al*. Genomic evolution and personalized therapy of an infantile fibrosarcoma harboring an *NTRK* oncogenic fusion. *JCO Precis Oncol* 2022; **6:** e2100283.

SUPPLEMENTARY MATERIAL ONLINE

Supplementary materials and methods

Table S1. Details of the antibodies used for immunohistochemistry

Table S2. Exact chromosome breakpoints and other details regarding the detected pathogenic aberrations

Table S3. Other genetic variants detected by the molecular genetic analysis

© 2024 The Authors. *The Journal of Pathology* published by John Wiley & Sons Ltd on behalf of The Pathological Society of Great Britain and Ireland. www.pathsoc.org

10969896, 2024, 1, Downloaded from https://pathsocjournals.onlinelibrary.wiley.com/doi/10.1002/path.6260 by Ukraine - Cochrane, Wiley Online Library on [11/12/2024]. See the Terms and Conditions (https://onlinelibrary.wiley.com/terms-and-conditions) on Wiley Online Library for rules of use; OA articles are governed by the applicable Creative Commons License